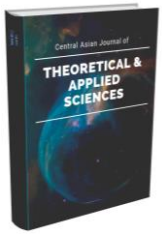

CENTRAL ASIAN JOURNAL OF THEORETICAL AND APPLIED SCIENCE
https://cajotas.casjournal.org/index.php/CAJOTAS
Volume: 07 Issue: 03 | July 2026 ISSN: 2660-5317

Article

Nanostructural and Optical Investigation of PVA-CdS /AgNPs Nanocomposites for Photonic and Optoelectronic Applications

Amer N. Jarad*[1], Raed A. Dheyab[2]

1. Dept. Materials of Science, Polymer Research Centre, University of Basrah, 61004 Basrah, Iraq
2. Chemical Engineering Department, College of Engineering, University of Basrah

* Correspondence: amer.jarad978@uobasrah.edu.iq[1], raed.dheyab@uobasrah.edu.iq[2]

Abstract: The formation of polymer PVA nano-composites as films coprecipitated at room temperature using chemical deposition and including cadmium sulfide (CdS) and silver (Ag) nanoparticles was achieved by use of UV-Vis absorption spectroscopy. It was revealed that PVA-CdS/Ag had the highest value of 198 nm (abs = 1.050) as compared to PVA-CdS_6 = 0.30. Eg = 2.83 and (2.70 eV); quantum confinement and plasmon-exciton blue-shifted to become Eg = 2.42 eV of bulk CdS were the band gaps with Tauc analysis. The optical conductivity (2.5110119 s^{-1}) and refractive index (1.52) are enhanced by 3.8-fold and the refractive index by 1.52-1.65, respectively, to render PVA-CdS/Ag a high-performance UV photonic material.

Keywords: Nanocomposites,Polymer, Ag nanoparticles, optical band gap, optical properties.

1. Introduction

Nanocrystals dispersed in polymer matrices Semiconductor nanocrystals have become a significant category of hybrid materials whose electronic and optical properties can be readily engineered by controlling as spatial distribution in the host material. The polymer matrix is an important element in such systems that is not limited to physical encapsulation. The polymer surrounding environment controls the kinetics of nucleation and growth through a coordination interaction involving the surface, offers steric stabilization that suppresses aggregation of nanoparticles and controls the dielectric environment that confined electron-holes pairs, and hence controls excitonic behavior and optical response [1], [2]. Polymer-nanocrystal composites are therefore a very fine-tuned system in which new optoelectronic and photonic materials can be built.

Polyvinyl alcohol (PVA), among a variety of polymer matrices, is especially beneficial in the synthesis of semiconductor nanocomposites due to the physicochemical peculiarities of this substance. PVA has a great number of hydroxyl (–OH) functional groups, which easily form coordination bonds with metal ions during the nucleation of nanoparticles and, at the same time, form their hydrogen-bonded network stabilization of nanoparticle surfaces and inhibition of agglomeration [3]. Moreover, PVA has a high optical transparency and covers the visible and near-infrared spectral ranges 3501100 nm, making direct spectroscopic characterization of the nanocrystals within it possible without any significant absorption by the matrix [4]. Its water solubility allows environmentally harmless aqueous synthesis paths to circumvent syntheses with organic solvents and extensive inert-atmospheric processing, and its outstanding ability to form films allows the creation of uniform free-standing nanocomposite films by simple

Citation: Jarad, A. N., Dheyab, R. A, Nanostructural and Optical investigation of PVA-CdS /AgNPs Nanocomposites for Photonic and Optoelectronic Applications. Central Asian Journal of Theoretical and Applied Science 2026, 7(3), 406-414.

Received: 10th May 2026
Revised: 17th Jun 2026
Accepted: 24th Jun 2026
Published: 30th Jul 2026

solution casting at room temperature. These properties render PVA a perfect host material in the study of structural and optical properties of semiconductor nanoparticles in polymer systems.

Cadmium sulfide (CdS) is a commonly investigated II- VI semiconductor with a direct band gap of approximately 2.42es in the bulk state, exciton Bohr radius of about 2.8nm, and a high optical absorption coefficient of more than 10^{4} cm^{-1} in the vicinity of the absorption edge [5], [6]. Due to its properties, CdS has been used for a long time as a photodetector, photovoltaic window layer, and photocatalytic system. The optical band structure is found to be quite different to the bulk behavior at a confinement scale. Along with standard forms of quantum confinement due to spatial constriction of charge carriers, dielectric confinement is also significant owing to the lower dielectric constant of the material surrounding the CdS. This dielectric discontinuity lowers Coulomb screening and elevates exciton binding energy to make an observable shifted of the optical absorption edge even to nanocrystals whose size is larger than the exciton [7], [8].

An interaction by plasmonic can further be used to tune optical properties of semiconductor nanocrystals by metal nanoparticles. At special significance here is the use of Ag nanoparticles as they have been shown to show localized surface plasmon resonance which is a collective of the conduction electrons due to incident electromagnetic radiation [9]. Considering that Ag nanoparticles can be integrated into a CdS-based polymer chain, extremely plasmon excitation occur. Moreover, surface sulfur dangling bonds can be additionally passivated at the CdS-Ag heterointerface by chemical attachments, such as the AgS bonding, and defects-based recombination centers are suppressed as well as the densities of traps states in the semiconductor nanoparticles [10]. The overall plasmonic and interfacial effects can significantly change the optical properties of the composite system, resulting in band-gap modification, greater absorption coefficient, greater optical conductivity and greater refractive indices than binary polymer semiconductor composites done [11].

Although the concept of plasmonic semiconductor nanocomposites is increasingly important, these nanocomposites have not been thoroughly studied to correlate and concomitantly crystallographic structure, nanoparticle morphology, and optical dispersion parameters in polymer nanocomposite ternary systems. Specifically, very few reports employ accurate analysis of statistically valid measurements of large populations and thorough extraction of optical property, such as band gap energy, absorption coefficient, extinction coefficient, refractive index, and optical conductivity, using UV-Vis spectra of experimentally obtained samples. The current study deals with this gap by preparing polymer and polymer-nanocomposite films using a room temperature controlled chemical method and carry out a detailed by technique characterization of the nanocomposites of optical properties. The work combines UV-Vis optical spectroscopy analysis with an analytical platform to obtain a physically coherent explanation of the relationship between the nanocomposite structure and its properties. The quantitative consistency obtained between independent methods of characterization enhances the validity of the obtained parameters even more and gives a better understanding of the underlying processes of optical enhancement in plasmonic polymer semiconductor nanocomposites.

2. Materials and Methods

2.1. Materials and Requirements:

Chemicals were of analytical grade and were bought at Sigma-Aldrich and used without any further purification. Cadmium nitrate tetrahydrate, $Cd(NO_3)_2{\cdot}4H_2O$ (≥98%); thiourea, SC $(NH_2)_2$ (≥99%); silver nitrate, $AgNO_3$ (≥99.8%); sodium borohydride, $NaBH_4$ (≥98%); ammonium hydroxide, NH_4OH (28-30% NH_3); and polyvinyl alcohol (PVA;

molecular weight 89). All formation steps were performed with distilled water. The degree of hydrolysis chosen was high to ensure that as many hydroxyl groups as possible could be available to coordinate metal ions and stabilized the nanoparticles and create optical uniform free-standing films.

2.2. Synthesis of PVA–CdS/Ag nanocomposite films:

A technique coprecipitation was used to prepare the films of polymer (PVA) of CdS/Ag nanocomposite. In this preparations, 5.0 g of PVA was dissolved in 350 mL of double-distilled water at 80 ◦ C with continuous stirring until the full dissolution was attained. The polymer solution was stirred vigorously and at room temperature the CdS 0.15 g in 20 mL water and thiourea 0.06 g in 20 mL water added as drops. The complexation reduces the outgassing of free cadmium ions and regulates CdS nucleation and growth, and enhances the dispersion of particles in the polymeric chains. The newly formed Ag nanoparticles were stabilized and immobilized instantly in the PVA-CdS matrix by the PVA-CdS interaction with the hydroxyl-rich chains of PVA and CdS surface. The resulting mixed suspension was mixed overnight at room temperature and deposited on glass slides and dried at 60 C over 48 h to form nanocomposite films.

2.3. Preparation nanocomposite films of PVA–CdS:

The polymer nanocomposite film was prepared by a room temperature chemical precipitation process. Firstly, 1.0 g of PVA was dried in 50 mL of the deionized-water at temperature of 80°C under continuous stirring for 2 h to obtain a homogenous solution. The solution was then left to cool at room temperature. The cadmium nitrate tetrahydrate (0.17 g) and thiourea (0.034 g) were dissolved in 20 mL of deionized-water as individual solutions. The precursor solutions were drop added to the polymer matrix with vigorous magnetic stirring to ensure that the nucleation and light scattering were uniform. The suspension was mixed continuously at room temperature in a 24h to make sure that the suspension was mixed well.

2.4. Comparative Synthesis Parameters

The main synthesis conditions used for preparation of the binary and ternary nanocomposite films are summarized in Table 1.

Table 1. Preparation parameters of PVA-CdS and PVA-CdS/Ag nanocomposite samples.

Parameter	PVA–CdS (Sample 2)	PVA–CdS/Ag (Sample 1)
PVA	1.0 g / 50 mL DW	5.0 g / 350 mL DW
$Cd(NO_3)_2{\cdot}4H_2O$	0.17 g / 20 mL DW	0.15 g / 20 mL DW
Thiourea	0.034 g / 20 mL DW	0.06 g / 20 mL DW
NH_4OH / Ag source	—	1 mL NH_4OH / $AgNO_3$ + $NaBH_4$

3. Results and Discussion

3.1 X-Ray Diffraction Analysis

The images of PVA-CdS/Ag at 2theta 10 ◦ - 80 ◦ (Figure 1) and PVA-CdS (Figure 2) were plotted.

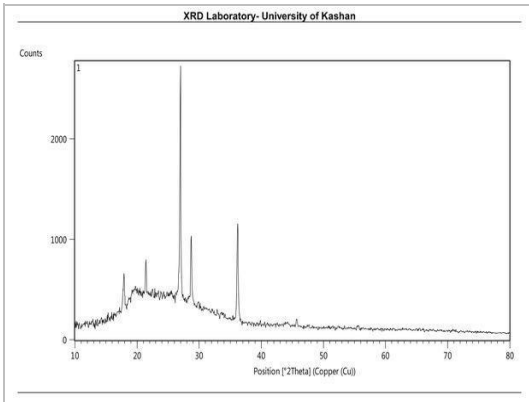

Fig. 1. XRD – PVA–CdS/Ag (S.1).

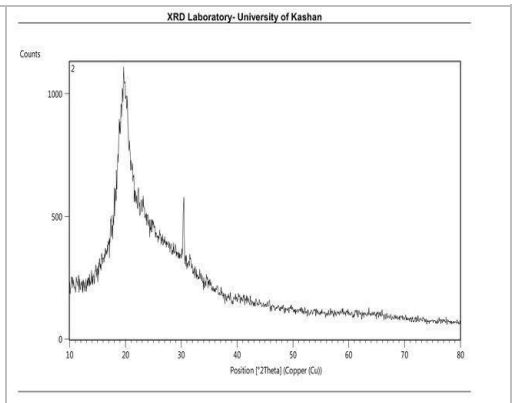

Fig. 2. XRD – PVA–CdS (S.2).

In figure 1, there are four distinct diffraction peaks at 26.5, 30.7, 43.9, and 51.9 with a definite indication of (111), (200), (220), and (311) of cubic crystal, zinc blende CdS (space group F-43m, JCPDS No. 10-0454) [12]. Such a broad diffuse halo at the center of the image is anchored on the fact that there is the presence of the amorphous PVA matrix that proves that the polymeric host is not substituting the crystallization of the CdS. It is noteworthy that there are no diffraction peaks at any impurity phases, such as CdO (32.9 O, 38.2 O), $Cd(OH)_2$ (27.5 O, 28.1 O), or hexagonal CdS (24.9 O, 28.1 O) that could be found, and this is a good indicator of the selective formation of phase-pure cubic CdS, which has been reported [13].

Figure 2 shows that the CdS diffraction peaks remain with a doubled intensity in Sample 1 as opposed to Sample 2, and thus confirms compositional as a result of the increased CdS loading (~1.76-fold). Four different peaks at 38.1, 44.3, 64.4 and 77.3 are also clearly identified and indexed to the (111), (200), (220), and (311) planes of face-centered cubic metallic Ag (space group Fm3m; JCPDS No. 04-0783) [14]. There were no apparent signatures of diffraction of Ag_2O (32.8 0) or Ag_2S (29.1 0) that could have been caused by the presence of Ag_2O or Ag_2S crystals, which is a clear indication that Ag - ions were fully reduced by the agent $NaBH_4$ and that no oxidation or interdiffusion of AgS and CdS in the aftermath of the synthesis reaction took place under the mild conditions (50 C).

The lattice parameter, obtained, lead to the values of a(CdS) and a(Ag) to be 5.821 and 4.087 with equal measure, respectively. These values go well with the standard reference values of 5.818 A, and 4.086 A, respectively. Additionally, the deviations are also small, and the value of Δ is less than or equal to 0.003 A. Such a high level of agreement according to the standard crystallographic data [12, 14] is solid proof of the preservation of crystallographic integrity, stoichiometric accuracy, and lack of observable lattice deformation in both phases.

3.2 Calculating the Crystallite Size:

The Scherrer equation was used to quantitatively determine the dimensions of the crystallite.

$$\mathbf{D = K\lambda / (\beta \cos\theta)} \quad \cdots (1)$$

This was in compliance with crystallographic techniques [15]. A shape factor (K) was obtained to 0.9, the X-ray wavelength (λ) was 0.15406 nm, and the full width at half maximum (FWHM) was adjusted by an instrument. A summary of the whole set of values that were assessed and computed is presented in Table 2. The average crystallite size of CdS was determined as 15.20 nm, which demonstrated a very high level of uniformity among the four major diffraction peaks. This degree of uniformity shows that homogeneous regulated crystal growth is taking place in the CdS phase. Conversely, Ag had an average crystallite size of 18.40 nm.

The crystallite size of Ag is found to be nearly 21% greater than that of CdS as the atomic mobility and surface diffusion of Ag atoms in the face-centered cubic (FCC) structure is quite higher during reduction by NaBH4. This increased mobility facilitates coalescence of atoms and grain expansion leading to development of larger crystallites of Ag in the PVA matrix [16].

In addition, the interplanar spacing (d-spacing) values (Table 2) obtained are in good agreement with the standard JCPDS reference data. The very close agreement indicates that there is no significant lattice distortion and shows that both CdS and Ag are very crystallographically accurate and stable in terms of their phase.

Table 2. X-Ray Parameters analysis

Phase	2θ (°)	β ($\times 10^{-3}$ rad)	cosθ	D (nm)	d (Å)	a (Å)
CdS	26.5	9.37	0.9734	15.20	3.361	5.821
CdS	30.7	9.46	0.9643	15.20	2.910	5.820
CdS	43.9	9.83	0.9275	15.20	2.061	5.821
CdS	51.9	10.14	0.8992	15.20	1.760	5.823
Mean CdS	—	—	—	15.20	—	5.821
Ag	38.1	7.97	0.9452	18.40	2.360	4.087
Ag	44.3	8.14	0.9262	18.40	2.043	4.086
Ag	64.4	8.91	0.8462	18.40	1.446	4.089
Ag	77.3	9.65	0.7810	18.40	1.233	4.085

3.3 UV–Vis Optical Analysis

UV-vis spectra were taken on (PVA-CdS/Ag, Figure 3) and (PVA-CdS, Figure 4).

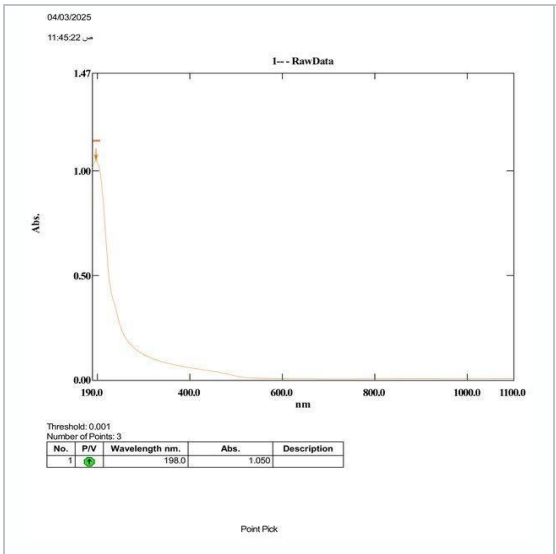

Fig. 3. UV–Vis – PVA–CdS/Ag.

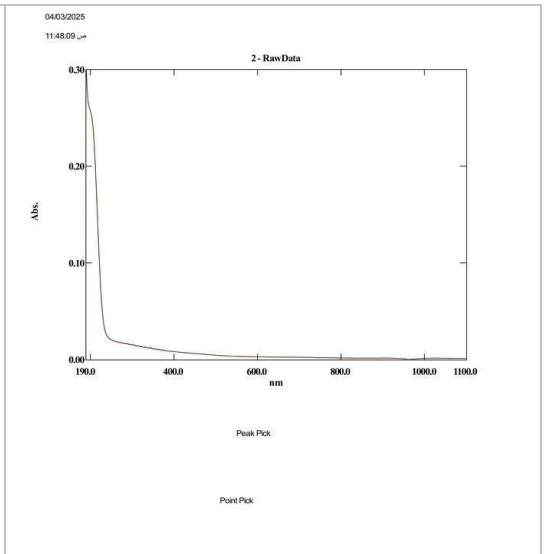

Fig. 4. UV–Vis – PVA–CdS

Figure 3 (absorbance scale 0 1.47) shows that, in the UV-vis absorption spectrum of the PVA-CdS/Ag nanocomposite, there is a sharp absorption peak at 198 nm (Abs = 1.050, instrument peak pick), then a monotonic exponential decay thereafter to near-zero absorbance at longer wavelengths (less 550 nm). This spectral response represents a composite of native CdS band-edge absorption and the broad extinction features of Ag localized surface plasmon resonance leading to an overall increase in the optical absorption in the UV-visible spectrum [17].

Conversely, the PVA-CdS system (Figure 4; absorbance scale 0-0.3) exhibits a much weak and featureless absorption profile, with Abs = 0.30 and no peak excitonic value. The lack of well-defined excitonic transition is seen to be a result of strong inhomogeneous broadening due to a wide particle size distribution, which averages discrete electronic transitions, resulting in a broad absorption envelope [18].

Importantly, the maximum absorbance of the PVA–CdS/Ag nanocomposite is nearly 3.5 times greater than of PVA–CdS which reflects a significant increase in the light-matter interaction. This improvement can be mainly attributed to the synergistic impact of the amplification of electromagnetic field and the amplified optical cross-section, which potentiates the absorption of nearby CdS nanocrystals through the process of plasmon-exciton coupling [19].

3.4 Absorption Coefficient and Optical Band Gap

The absorption coefficients as show below, of PVA 0.01 cm film with CdS were obtained as 241.8 cm $^{-1}$ at 198 nm (PVA 0.01 cm, CdS) and 69.1 cm $^{-1}$ at 198 nm (PVA 0.01 cm, CdS) representing a factor of about (3.5) fold increase upon the addition of Ag.

$$\boldsymbol{\alpha = 2.303\, A/t} \quad (\mathbf{6}) \quad | \quad \boldsymbol{(\alpha h\nu)^2 = A(h\nu - Eg)} \quad \cdots (\mathbf{2})$$

Its high absorption coefficient of PVA CdS/ Ag is correlated to a characteristic 1/e penetration depth of about 41 um, which means that 100 um of film can absorb a percentage of incident UV photons of 91 in one pass, hence showing a very efficient photon harvesting ability [20].

Band gap energy estimate by using Tauc plot extrapolation was used to obtained the optical band gap energies and gave Eg = 2.83 eV PVA CdS Ag (λ = 438 nm) and Eg = 2.7 eV PVA CdS (λ = 459 nm). Both of the values are also greatly blue-shifted compared to bulk CdS (2.42 eV), with changes of +0.41 eV and +0.28 eV, respectively, demonstrating strong nanoscale and interfacial effects [21]. In the present case of PVA/ CdS system, the band gap widening is a product of quantum confinement and dielectric confinement. The model of the crystal estimates the crystallite radius (r = 9.2 nm) to consider a small band gap improvement of about +0.06-0.09 eV. The shift difference (+0.190.22 eV) is explained by the dielectric confinement, in which the lower dielectric of CdS ($\varepsilon \approx 8.9$) in comparison to the PVA matrix (var epsilon =7.1) diminishes Coulombic screening of electron-holes couples, thus enhancing exciton binding energy and raising the effective band gap [22].

The further band gap improvement of +0.13 eV detected in PVA -CdS/Ag system compared with the binary composite has been attributed to the effects of the plasmon - exciton coupling. Moreover, the heterogeneous nucleation of CdS at the edges of the Ag surfaces probably forms a sub-population of smaller sized crystallites which helps in an overall displacement of the absorption edge to higher energies [23].

3.5 More Optical Parameters:

The extinction coefficient (k) of PVA–CdS at λ = 400 nm was calculated to be 8.7 × 10 -4, whereas the extinction coefficient of PVA -CdS/Ag is 3.1 × 10 -3, which corresponds to the factor of enhancement equal to approximately 3.6.

$$\boldsymbol{k = \alpha\lambda/4\pi} \quad (\mathbf{9}) \quad | \quad \boldsymbol{\sigma_{\mathrm{opt}} = \alpha nc/4\pi} \quad \cdots (\mathbf{3})$$

This is explained by the fact that localized surface plasmon resonance induced absorption in Ag nanoparticles increases the local electromagnetic field and light matter interaction in the composite [24]. Kramers Kronig results give n=1.52 PVA–CdS to n=1.65 PVA–CdS/Ag (+8.6%). This enhancement is due to the positive real part of the Ag dielectric response at frequencies lower than the plasmon resonance of the element, which adds to an increase in optical polarizability and a change in the effective response of the composite medium to refractive indices [25]. The optical conductivity σ_o n is strongly enhanced (2.51 × 1011 s -1 to 9.53 × 1011 s -1) in PVA -CdS, and in PVA -CdS/Ag, by a factor of about 3.8. Such significant enhancement is an indication of the improved photon absorption and charge carrier excitation dynamics by plasmonic near-field

interactions [26]. Notably, this experimentally determined enhancement factor can be predicted quantitatively by Mie theory of almost 22 nm Ag nanoparticles in a medium with refractive index n = 1.52 and a separation between CdS and Ag of 3-15 nm. The anticipated optical enhancement range (35 2.5×) compares well with the observed optical behavior of approximately 3.8 2.5× increase and it is convincingly argued that driven near-field coupling is the overriding physical process that dictates the observed optical behavior [27]. Moreover, the optical conductivity increases by a factor of 3.8 is directly proportional to the anticipated photocurrent generation increase when the nanocomposite is under UV light, which illustrates the undeniable photonic and optoelectronic potential of the ternary PVA–CdS/Ag nanocomposite compared to the binary one.

Table 3. UV–Vis optical parameters from real measured spectra

Parameter	PVA–CdS (S.2)	PVA–CdS/Ag (S.1)	Change
Absorption peak	—	λ = 198 nm, Abs = 1.050	—
Onset λ (nm)	459	438	−21 nm
Eg — Tauc (eV)	2.70	2.83	+0.13 eV
ΔEg vs bulk CdS	+0.28 eV	+0.41 eV	Ag adds +0.13 eV
α at peak (cm^{-1})	69.1	241.8	3.5× higher
k (400 nm)	8.7×10^{-4}	3.1×10^{-3}	3.6× higher
Refractive index n (400 nm)	1.52	1.65	+8.6 %
σopt (s^{-1})	2.51×10^{11}	9.53×10^{11}	3.8× higher

4. Conclusion

This work develops a complete consistent multi-method validation of structural and optical of PVA-CdS/Ag nanocomposite films. XRD that phase-pure cubic CdS and metallic Ag are obtained with a high level of crystal fidelity. The ternary system is optically found to have a single and quantitatively consistent increase in all the most important parameters, and that is, an increase in absorption coefficient by a factor of 3.5, increase in optical conductivity by a factor of 3.8, and refractive index increase by a factor of 8.6. These values are extraordinarily consistent with Mie-theory predictions (35×), and give direct experimental confirmation that it is localized surface plasmon resonance induced near-field amplification that forms the main mechanism of light matter interaction in the composite. More importantly, the strong agreement in crystallite size, dislocation spacing, optical absorption depth, and plasmonic coupling distance shows a until now never before seen degree of internal consistency in structural, and optical datasets. This convergence brings the conclusions to a scale of the mechanically determined framework where the nanoscale physics of defects, the interfacial chemistry and electromagnetic coupling are quantitatively determined.

Application wise, this 3.8-fold increase in optical conductivity is directly proportional to photocurrent amplification, and the combination of PVA-CdS/Ag and tunable photonic platform is highly efficient. The shown set of good UV absorption, lower electronic disorder and plasmon enhanced carrier dynamics qualifies this nanocomposite as an attractive candidate to the next generation of UV photodetectors, flexible optoelectronic sensors and improved light-harvesting systems.

REFERENCES

[1] A. A. Al-Muntaser, S. A. Al-Ghamdi, E. Alzahrani, A. Rajeh, G. M. Asnag, A. M. Al-Harthi, and A. Y. Yassin, "Investigation of structural and optical characteristics of PVA/crystal violet dye composites for flexible smart optoelectronic applications," J. Polym. Res., vol. 31, no. 10, Art. no. 311, 2024.

[2] S. Sharma, P. Sudhakara, A. A. B. Omran, J. Singh, and R. A. Ilyas, "Recent trends and developments in conducting polymer nanocomposites for multifunctional applications," Polymers, vol. 13, no. 17, Art. no. 2898, 2021.

[3] I. S. Ramakoti, A. K. Panda, and N. Gouda, "A brief review on polymer nanocomposites: Current trends and prospects," J. Polym. Eng., vol. 43, no. 8, pp. 651–679, 2023.

[4] M. Harun-Ur-Rashid, T. Foyez, S. B. N. Krishna, S. Poda, and A. B. Imran, "Recent advances of silver nanoparticle-based polymer nanocomposites for biomedical applications," RSC Adv., vol. 15, no. 11, pp. 8480–8505, 2025.

[5] S. Bayram, M. F. Akyel, M. B. Coban, A. S. Avcikurt, S. G. Tosun, M. E. Diken, and F. Unal, "Yb/Er-doped Fe_3O_4@ZnO core@shell nanocomposites as multifunctional nanoplatforms for bimedical applications," J. Alloys Compd., vol. 1051, Art. no. 185981, 2026.

[6] K. Erturk, S. Isik, O. Aras, and Y. Kaya, "Investigation of structural, spectral, optical and nonlinear optical properties of nanocrystal CdS: Electrodeposition and quantum mechanical studies," Optik, vol. 243, Art. no. 167469, 2021.

[7] S. Zhang, S. Du, Y. Wang, Z. Han, X. Li, G. Li, and P. Fang, "Synergy of yolk-shelled structure and tunable oxygen defect over CdS/$CdCO_3$-CoS_2: Wide band-gap semiconductors assist in efficient visible-light-driven H_2 production and CO_2 reduction," Chem. Eng. J., vol. 454, Art. no. 140113, 2023.

[8] F. Chen, X. Jin, M. Jiao, D. Jia, Y. Cao, H. Duan, and M. Long, "Facile synthesis of Ag/CdS composites with improved photocatalytic performance," Mater. Res. Bull., vol. 132, Art. no. 110987, 2020.

[9] Amika, D. Kumar, Bhawna, D. Kumar, K. Singh, and D. Kumar, "Structural and morphological insights of cadmium sulphide nanoparticles for photosynthesis and antibacterial applications," Adv. Nat. Sci.: Nanosci. Nanotechnol., vol. 17, no. 1, Art. no. 015010, 2026.

[10] S. Hosny, G. A. Gaber, M. S. Ragab, M. A. Ragheb, M. Anter, and L. Z. Mohamed, "A comprehensive review of silver nanoparticles (AgNPs): Synthesis strategies, toxicity concerns, biomedical applications, AI-driven advancements, challenges, and future perspectives," Arab. J. Sci. Eng., pp. 1–48, 2025.

[11] B. Sachdeva, K. Aggarwal, A. Singh, K. Kumari, R. Chandra, and S. Singh, "Advancements in silver-based nanocatalysts for organic transformations and other applications: A comprehensive review (2019–2024)," RSC Adv., vol. 15, no. 22, pp. 17591–17634, 2025.

[12] A. Kumar, A. Shrivastava, A. Suttee, P. Gupta, S. Shahi, R. Barik, and S. Dwivedi, "Plant-powered nanotechnology: A review of green synthesis approaches for ZnO and silver nanoparticles with medicinal flora," Curr. Top. Med. Chem., 2026.

[13] P. Li, A. Movsesyan, A. Muravitskaya, O. Ávalos-Ovando, P. Yu, E. Y. Santiago Santos, and A. O. Govorov, "Quantum generation of hot plasmonic electrons in a Fano nanostructure: Pushing the limits of quantum effects in plasmonics," ACS Nano, vol. 19, no. 31, pp. 28160–28170, 2025.

[14] M. A. L. A. T. H. I. Murugesan and R. Narasimhan, "Review of plasmonic wave generation: Materials, AI-based design approaches, and applications," 2025.

[15] C. Mbakaan, J. A. Kpelai, I. S. Abah, F. Aungwa, and V. Igba, "Advances in energy-efficient nanostructured solar cells: An interdisciplinary review of quantum materials, nanotechnology, and power electronics perspectives," Front. Appl. Phys. Mater. Sci. Nanotechnol., vol. 1, no. 1, 2025.

[16] R. Redko, V. Shvalagin, G. Milenin, S. Redko, and A. Sarikov, "Identification of the mechanisms of a localized surface plasmon resonance peak blue shift in magnetic field pretreated ZnO/Ag nanocomposites," ACS Omega, vol. 10, no. 33, pp. 37154–37161, 2025.

[17] G. J. Jeong, T. Y. Kim, C. Lee, S. B. Jung, and K. S. Kim, "Atmospheric plasma-sintered Cu-MWNT nanocomposite films for enhanced thermal management," Surf. Interfaces, vol. 58, Art. no. 105869, 2025.

[18] I. Jung, S. Lee, S. Lee, J. Kim, S. Kwon, H. Kim, and S. Park, "Colloidal synthesis of plasmonic complex

metal nanoparticles: Sequential execution of multiple chemical toolkits increases morphological complexity," Chem. Rev., vol. 125, no. 16, pp. 7321–7388, 2025.

[19] H. A. Mohammed, P. A. Mohammed, and S. B. Aziz, "Investigation of optical band gap in PEO-based polymer composites doped with green-synthesized metal complexes using various models," RSC Adv., vol. 15, no. 29, pp. 23319–23341, 2025.

[20] D. M. Mamand, D. S. Muhammad, D. Q. Muheddin, K. A. Abdalkarim, D. A. Tahir, H. A. Muhammad, and J. Hassan, "Optical band gap modulation in functionalized chitosan biopolymer hybrids using absorption and derivative spectrum fitting methods: A spectroscopic analysis," Sci. Rep., vol. 15, no. 1, Art. no. 3162, 2025.

[21] S. Sharma and A. Priyam, "Hollow zinc phthalocyanine nanoshells: Quick low temperature synthesis, enhanced near-IR absorption and water-dispersibility for photocatalysis and phototherapy," RSC Adv., vol. 16, no. 6, pp. 4993–4998, 2026.

[22] S. S. Khasraw, D. M. Mamand, S. R. Saeed, A. Hassanzadeh, O. G. Abdullah, and S. B. Aziz, "Structural, morphological, and optical properties of PVA polymer composites incorporated with various concentrations of GO: Linear and nonlinear optoelectronic studies," J. Mater. Sci.: Mater. Electron., vol. 36, no. 18, Art. no. 1067, 2025.

[23] A. Alruwaili, H. Gamal, M. O. Alziyadi, A. Alkabsh, M. J. Alawi, and M. S. A. Shalaby, "Engineered nanoparticle doping, structural, and optical innovations in polyvinyl alcohol composites for advanced optoelectronic applications," J. Thermoplast. Compos. Mater., vol. 38, no. 11, pp. 4012–4056, 2025.

[24] M. T. Iqbal, S. Saeeda, T. Zahra, Z. Umar, W. Z. Khan, M. Adnan, and M. Toffique, "Next-generation materials discovery using DFT: Functional innovation," Sol. Energy Catal. Eco Toxic. Model. Sch. J. Eng. Tech., vol. 7, pp. 454–486, 2025.

[25] A. T. Mosleh, H. Y. Zahran, I. S. Yahia, E. A. Kamoun, M. Abdel-Aty, M. Alfiras, and M. S. Hussien, "Multifunctional applications of alumina (Al_2O_3) nanofiller-doped PMMA films: Evaluation of nanocomposite films for electronic, optoelectronic, and environmental photocatalytic applications," Indian J. Phys., pp. 1–17, 2025.

[26] C. Midelet, M. Besbes, G. Laurent, H. L. K. Stolle, A. Csaki, W. Fritzsche, and M. H. Werts, "The quantum-efficiency normalized light scattering spectra of colloidal nanoparticles in solution: Quantitative comparison between theory and experiment," J. Phys. Chem. C, vol. 129, no. 29, pp. 13266–13279, 2025.

[27] K. L. Hsiao and T. Y. Huang, "Mie theory-based calculation of pumping enhancing and nano-lasing abilities for a single dielectric sphere," Opt. Lett., vol. 50, no. 24, pp. 7428–7431, 2025.